ELSEVIER

Journal of Nuclear Materials 296 (2001) 219–224

journal of nuclear materials

www.elsevier.com/locate/jnucmat

A study on martensitic and austenitic steels after exposure in mercury at 573 K up to 5000 h

R.Kh. Zalavutdinov [a,*], Y. Dai [b], A.E. Gorodetsky [a], G.S. Bauer [b], V.Kh. Alimov [a], A.P. Zakharov [a]

[a] *Institute of Physical Chemistry, Russian Academy of Sciences, Leninsky pr. 31, 117915 Moscow, Russia*
[b] *Paul Scherrer Institut, CH-5232 Villigen PSI, Switzerland*

Abstract

The chemical composition, structure and morphology of surface layers formed on stressed martensitic (F82H, MANET-II) and austenitic (316L) steel samples after exposure in static mercury with air or Ar inside the containers for 5000 and 2000 h, respectively, at 573 K have been studied by different surface analysis techniques (electron probe microanalysis (EPMA), scanning electron microscopy (SEM), reflected high energy electron diffraction (RHEED), X-ray diffraction (XRD), and secondary ion mass spectrometry (SIMS)). It has been shown that all three steels are oxidized (oxide thickness greatest on F82H and least for 316L) and covered with red HgO single crystals when air is present in the system. The oxidation of the steels and Hg can be suppressed by using Ar in the containers. Cracks have been found only at the notch roots of the 316L samples. There is no evident Hg corrosion observed.

1. Introduction

For next generation pulsed spallation sources, such as the European Spallation Source (ESS) and the American Spallation Neutron Source (SNS), liquid mercury (Hg) is considered as the best target material [1]. The main advantages are that, firstly, compared to lead-bismuth (Pb–Bi), Hg is the preferred target material for short-pulsed neutron source due to its high thermal neutron absorption cross-section [2]; secondly, Hg is liquid at room temperature, which does not need heating to avoid freezing like in the Pb–Bi case; finally, Hg is expected to have less soak corrosion effects on structural materials than Pb–Bi [3].

The structural material of the beam window of a liquid metal target container will be irradiated under proton and neutron mixed spectrum. Although the behavior of structural materials under this type of irradiation is still not clear yet, neutron irradiation experience with austenitic steel suggests 316L is a suitable container material for SNS [4] where the temperature at the beam window will be about 473 K. For ESS target, martensitic steels have been selected as the container material [5] since the higher power (5 MW against 2 MW for SNS) will give higher temperature, about 573 K, and higher thermal mechanical load.

It is well known that liquid metal corrosion and embrittlement will be critical issues for a liquid metal target. Hg corrosion on both austenitic steels and martensitic steels has been studied at temperatures above 673 K in 1960s [6,7]. The significance of corrosion effects in a lower temperature range is little known though the preliminary results show there might be no serious corrosion [8,9].

The present work is aimed to study the situation at the beam window of the ESS target container, namely the temperature around 573 K and the mechanical load up to 200 MPa. The materials selected are martensitic steels, F82H and MANET-II. They have 7.7% Cr and 10.3% Cr, respectively, and may show different Hg corrosion behaviors. For a comparison, 316L stainless steel has been tested under similar conditions.

* Corresponding author. Tel.: +7-095 330 2192; fax: +7-095 334 8531.
E-mail address: rinad@ipc.rssi.ru (R.Kh. Zalavutdinov).

0022-3115/01/$ - see front matter
PII: S0022-3115(01)00546-3

Table 1
Chemical composition of the tested steels in wt% [9]

Steel	Cr	Ni	Mn	Mo	W	Nb	Ta	V	C	Si	Fe
F82H	7.65	–	0.50	–	2.0	–	0.04	0.18	0.09	0.09	Bal.
MANET-II	10.3	0.62	1.22	0.57	–	0.14	–	0.20	0.11	0.27	Bal.
316L	17.4	12.7	1.56	2.56	–	–	–	–	0.02	0.4	Bal.

2. Experimental

The chemical compositions of F82H, MANET-II and 316L steels are given in Table 1. C-ring type samples, with and without notches, have been used in static Hg corrosion tests [9]. Sketches and dimensions of the C-ring samples are shown in Fig. 1(a). The notches were prepared with a milling machine. All samples were electro-polished and cleaned in alcohol in an ultrasonic bath. The samples were tested without any heat treatment. The maximum stresses at the outer surface were about 200 MPa (316L and MANET-II) and 300 MPa (F82H) applied by compressive deforming of the samples before the tests (Table 2). The tests were performed in experimental setups (Fig. 1(b)) at 573 K and divided into two batches. In Batch 1, samples were put into Hg with air inside the containers and in Batch 2 with about 2 bar pure (99.99%) Ar gas. The containers with air reached 5000 h and those with Ar reached 2000 h.

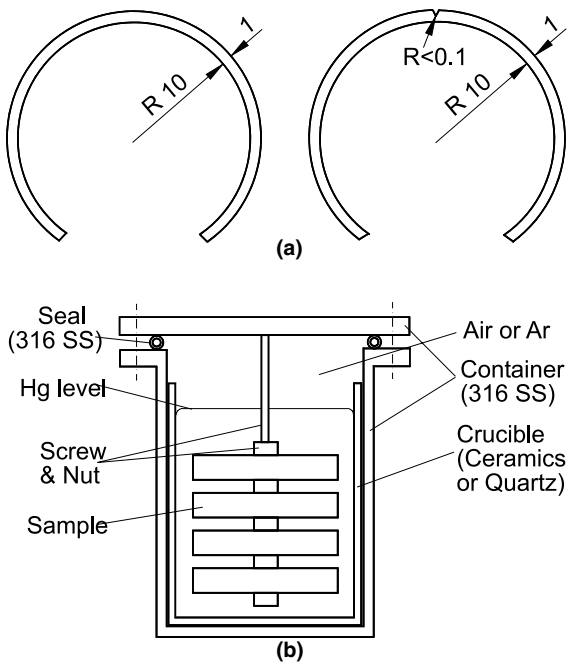

Fig. 1. (a) Sketch of smooth and notched C-ring type samples. The width of the samples is 5 mm. The depth of the notch is about 0.5–0.6 mm. (b) Sketch of experimental setup. Note: samples, the screw and nuts are always of the same kind of material.

After corrosion tests, the samples were mechanically cut into three equal parts. The central part of each sample was cleaned in alcohol in an ultrasonic bath and was analyzed by different surface analysis techniques. The chemical composition and morphology of the sample surfaces were investigated by the electron probe microanalysis (EPMA) and the scanning electron microscopy (SEM). Some samples were additionally studied by the X-ray diffraction (XRD), reflected high energy electron diffraction (RHEED) and secondary ion mass spectrometry (SIMS) for depth profiling.

3. Results and discussion

The analysis of the composition, morphology and structure of the surface layers formed on the samples after the corrosion tests allowed to establish some features of interface reactions for combinations of air/Hg/steel and Ar/Hg/steel at 573 K. The steels tested did not chemically react with Hg because no intermetallic compounds have been found containing Hg. Some red HgO single crystals were present on the samples, but most of them peeled off during cutting and ultrasonic cleaning. The breakdown of the surface layers was mainly caused by interaction of oxygen, coming through the stagnant Hg to the sample, with the steel.

3.1. Batch 1 (with air)

Optical and SEM inspections of the sample surfaces after corrosion tests disclosed that colour and morphology of the surfaces depended on the chemical composition of the steels. The F82H (Fig. 2(a)) and MANET-II (Fig. 2(b)) samples had black colour and a surface roughness about 1 μm. In contrast to this, the surfaces of the 316L (Fig. 2(c)) samples had gray colour and were smooth. Surface irregularities of martensitic steels consisted of thick iron oxide films and red HgO single crystals. Although the 316L samples had a weak oxidation attack, a few cracks with length of 5–30 μm at the notch root (Fig. 2(d)) were observed. Pittings in Fig. 2(c) were formed during electro-polishing of the samples.

Table 2
The list of the samples and their corrosion conditions

Sample	Material	Corrosion conditions
A1, smooth	316L	5000 h, air, 230 MPa[a]
B1, notched	316L	5000 h, air, 220 MPa
C1, smooth	F82H	5000 h, air, 300 MPa
D2, notched	F82H	5000 h, air, 210 MPa
E2, smooth	MANET-II	5000 h, air, 200 MPa
F2, notched	MANET-II	5000 h, air, 200 MPa
A3, smooth	316L	2000 h, Ar, 220 MPa
B3, notched	316L	2000 h, Ar, 200 MPa
C4, smooth	F82H	2000 h, Ar, 200 MPa
D4, notched	F82H	2000 h, Ar, 200 MPa

[a] '5000 h, air, 230 MPa' means that the sample was in Hg for 5000 h with air inside the container and the maximum stress at the outer surface was 230 MPa. For the notched samples the maximum stress was at the notch root.

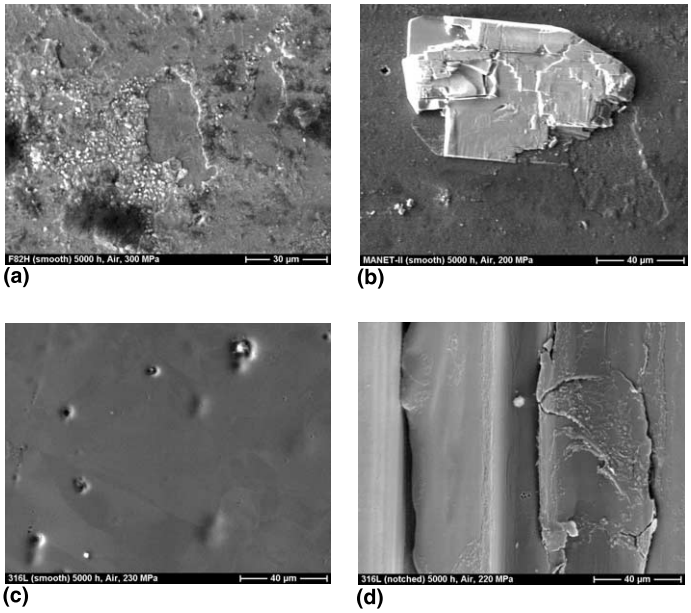

Fig. 2. SEM micrographs show morphology of C1 (F82H) (a) E2 (MANET-II) (b) and A1 (316L) (c) samples after 5000 h exposure in Hg with air inside the containers at 573 K. The difference in corrosion attack can be seen: (a) in the centre, a HgO crystal peeled off and the area is surrounded with the thick iron oxide layer; (b) HgO single crystal on the outer sample surface; (c) pittings formed during electro-polishing with TiC inclusions; (d) cracks at the notch root of B1 (316L) sample.

EPMA showed that all samples were oxidized and the oxide thickness decreased with increasing alloying element concentration. The oxide film thickness was calculated by a Multifilm code, using oxygen data and Fe_3O_4 and Fe_2O_3 oxides with density of 5.18 and 5.25 g/cm^3, respectively. The code is based on the use of $\phi(\rho z)$ curves according to Yakovitz–Newbury [10]. The maximum oxide thicknesses on the martensitic steels reached 680 nm for F82H and 310 nm for MANET-II. It should be noted that the places where HgO crystals were peeled off (Figs. 2(a) and (b)) were covered with thin oxide film of about 30 nm for both the martensitic steels. On the 316L samples, the thickness of oxide film varied in a range from 5 to 80 nm. No effect of applied stress level on oxidation of the steels was observed.

XRD was applied for analysing oxidized surface layers. The thicknesses of oxide films were thin enough for XRD analysis. Therefore, the intensities from oxides were low and comprised only (3–5)% intensities from the main bulk elements (Fig. 3). However, the oxides like α-Fe_2O_3 and Fe_3O_4 with crystallite size of 10–30 nm were determined. It is known [11] that oxides on surfaces of Fe–Cr steels are enriched with Cr during oxidation in air at elevated temperatures. In our XRD analysis the

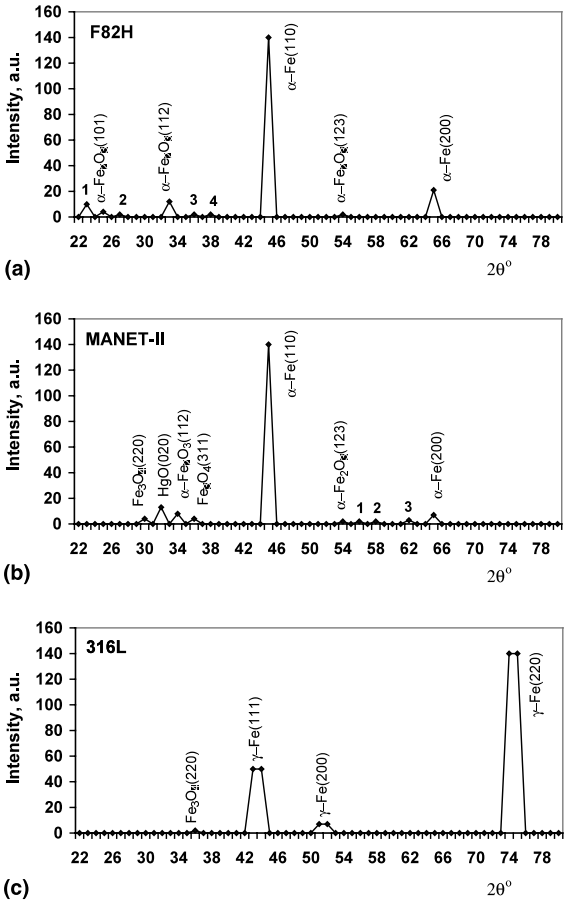

Fig. 3. XRD intensities from C1 (F82H) (a), E2 (MANET-II) (b) and A1 (316L) (c) samples after 5000 h exposure in Hg with air inside the containers at 573 K. The possible diffraction lines indicated by figures may be related with the following oxides: (a) 1 – $FeCrO_3$ (1 0 1); 2 – HgO (0 0 1); 3 – Fe_3O_4 (3 1 1); α-Fe_2O_3 (1 0 1); 4 – Fe_3O_4 (2 2 2); HgO (1 2 0); (b) 1 – Fe_3O_4 (4 2 2), α-Fe_2O_3 (1 2 3), Cr_2O_3 (1 1 6); 2 – Fe_3O_4 (5 1 1), α-Fe_2O_3 (2 3 3), HgO (0 2 1); 3 – Fe_3O_4 (4 4 0), α-Fe_2O_3 (1 0 3), Cr_2O_3 (1 2 4), HgO (0 2 2).

separation of Fe_2O_3 and $(FeCr)_2O_3$ or Fe_3O_4 and $FeCr_2O_4$ was impossible. The fraction of oxide-like spinal (Fe_3O_4, $FeCr_2O_4$, etc.) in the surface layers increased and the oxide film thickness decreased with the increase of alloying element concentration in the steels tested.

The F82H and MANET-II samples were also investigated by RHEED but it did not give any useful information about structure of the oxide films because the diffraction patterns contained only 2–3 diffuse halos. It is a typical situation for rough surfaces with ridges (~100 nm thick) covered by amorphous oxides with a thickness of 10 nm. In RHEED an angle between the primary electron beam and the sample surface is about 4° and the secondary diffraction beam is absorbed by accidental ridges.

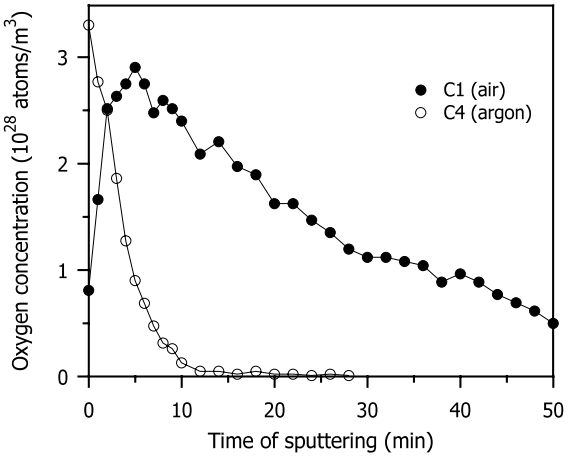

Fig. 4. The depth profiles of oxygen concentration in the samples of F82H determined with SIMS analysis. Sputtering time of 1 min corresponding to a depth of 9 nm.

A depth concentration profile of oxygen in the F82H sample (C1) was determined using SIMS measurement of O^- signal in the course of surface sputtering, as shown in Fig. 4. The profile can be characterized as a gradual decrease of oxygen with depth. The averaged thickness of oxide film was estimated to be about 500 nm. The presence of FeO^+ line in SIMS spectrum confirmed the formation of iron oxide on the sample surface. Additionally, the secondary ion species Hg^+ and HgO^+ were observed in the spectra.

Simultaneously with the formation of the oxide layers, the red HgO single crystals up to 1 mm large appeared on the steel surfaces (Figs. 2(b) and 5). The red HgO crystals have rhombohedral type of cells with lattice parameters: $a = 0.6121$ nm, $b = 0.552$ nm and $c = 0.352$ nm [12]. The areal density of HgO crystals on the Hg/steel interface increased with decreasing of alloying element concentration in the steels. The HgO crystals have faceted surfaces (Figs. 2(b) and 5(b)). The areal densities of small HgO crystals with size of 1–100 μm on the F82H (Fig. 5(a)) and MANET-II (Fig. 5(c)) samples were about 4×10^4 and 4×10^3 HgO/cm^2, respectively. The areal densities of large HgO crystals with size of 0.1–1 mm was ~500 HgO/cm^2. Fig. 5(d) shows a large HgO crystal on the notched MANET-II sample (F2).

3.2. Batch 2 (with Ar)

Optical and SEM inspections of the F82H and 316L samples after corrosion tests revealed that all surfaces were mainly smooth. The cracks were observed only at

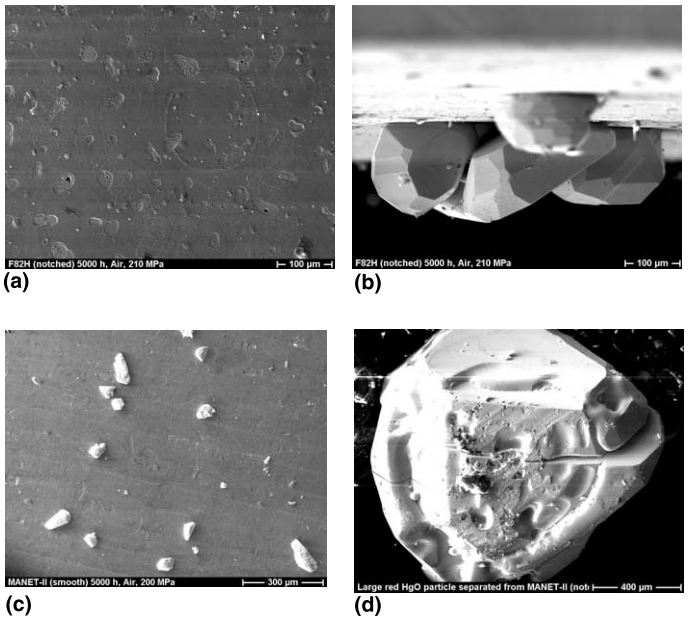

Fig. 5. SEM micrographs show morphology of different HgO crystals grown on the interface of Hg/martensitic steel after 5000 h exposure in Hg with air inside the containers at 573 K: (a) the iron oxide layer with traces of HgO crystal peeled off (sample D2, F82H); (b) a set of HgO single crystals on the inner surface (sample D2, F82H); (c) alignment of HgO crystals on the outer surface (sample E2, MANET-II); (d) a large HgO crystal separated from the sample F2 (MANET-II). One can see a few small Hg droplets on the crystal surface.

the notch root of the 316L samples. No HgO crystal was seen on the samples.

SIMS (Fig. 4) and EPMA showed that the samples were oxidized and the oxide film thickness was about 10 nm for F82H and 2 nm for 316L. The species Hg^+ and HgO^+ were not observed in SIMS analysis on an F82H sample (C4).

Thus, the main results of Hg/steel interface investigation show that at 573 K oxygen penetrates through Hg of some centimeters thick and reacts with the sample surfaces. It is proposed that at 573 K oxygen dissolves in Hg and diffuses in the bulk of Hg towards the samples [9]. Here, we have a specific case of 'inner oxidation' for a two-phase system (Hg and steel). Perhaps, along the boundaries between the specimens and their holders and liquid mercury a flux of air molecules exists and it can assist to steel oxidation. But we saw that HgO crystals were fixed at steel surface and grew normally to the surface towards mercury. They had faces with low index planes. Usually, such crystals grow from solutions [13]. Therefore, we assume that HgO crystals grew from oxygen saturated liquid mercury.

It is well known [14] that Hg can absorb oxygen at 570–620 K and then regenerate it at lower temperatures. One of the possible oxygen sorption mechanisms is a capture of negative oxygen ion (radius 0.132 nm) by a vacancy in liquid mercury (radius 0.181 nm) with formation of a HgO dynamic complex. Accordingly to our estimation, taking into account the vacancy formation energy of 0.2–0.3 eV, vacancy concentration at 573 K is equal to 0.1–1 at.% that in two orders of magnitude higher than vacancy concentration at 293 K. HgO complexes are mobile enough in liquid metal. The main impurity atoms in liquid mercury have a diffusion coefficient of 10^{-5}–10^{-4} cm^2/s [15]. So, taking the vacancy concentration (1 at.%), the oxygen diffusion coefficient (10^{-5} cm^2/s) and typical length (1 cm) into account, the oxygen diffusion flux towards steel surface was about 3×10^{15} O atoms/cm^2 s.

The preferable places for HgO nucleation were the oxidized steel surfaces. The XRD data showed that oxides formed on the steels investigated had different structures, depending on steel chemical composition. It is likely that on F82H steel covered with Fe_2O_3 the HgO nucleation occurs easier than on 316L and MANET-II steels that were covered with Fe_3O_4 and mixture of Fe_3O_4 and Fe_2O_3, respectively. At the same time the HgO nucleation on the air/Hg interface is made difficult by exchange fluxes of Hg and O atoms between liquid metal and gas phases (Hg partial pressure at 573 K is equal to 3.3×10^4 Pa). The simultaneously growing steel oxides and HgO crystals fixed on their surfaces relieve an oxygen oversaturation of Hg and provide the oxygen flux towards specimens.

There are data [11,16] on the oxidation of Fe–(7–8)% Cr steels in air. At normal pressure the thickness of oxide layer (h) increases with time (t) according to a parabolic law

$$h = Q/\rho = \sqrt{kt},$$

where Q is the oxide mass, ρ is the oxide density, and k is the oxidation rate constant ($k \approx 4 \times 10^2 \times \exp(-36\,000/\mathrm{RT})$ $\mathrm{g^2/cm^4}$ h). At 573 K after 5000 h exposure in air the thickness of oxide film can reach 0.3–0.6 μm. Such a thickness of oxide films was revealed in our experiments but it should be noted that the samples were put into Hg. The oxidation rate of Fe–(7–8)% Cr steels in air and in Hg practically is the same because the oxidation rate is limited by diffusion of metal cations through oxide.

So, the presence of oxygen in the system can give rise to formation of thick oxide layers on the martensitic steels and too much HgO single crystals. The former can reduce the heat transfer between Hg and the container and the latter may result in plugging. Of course these problems can be avoided by controlling the oxygen content in the system, for example, using inert gases, as shown by the results of Batch 2.

4. Conclusions

Corrosion tests on martensitic steels, F82H and MANET-II, and austenitic steel 316L, were conducted in static Hg at 573 K in two batches: (1) the Hg covered with air for 5000 h, and (2) the Hg covered with Ar for 2000 h. Different techniques (EPMA, SEM, RHEED, XRD, and SIMS) have been applied for the surface analysis. The main results show that the surfaces of the samples are oxidized and covered with a large amount of red HgO single crystals (1 μm to 1 mm) when air exists in the system. The surface layers formed in the presence of air consist of a set of oxides Fe_3O_4, Fe_2O_3 and Cr_2O_3 and have a thickness up to 680 nm for F82H, 310 nm for MANET-II and 80 nm for 316L. Displacing air with Ar in the containers can drastically reduce the oxidation of the steels. In this case the maximum thickness of oxide film is of 10 nm and no HgO crystals form. For both batches of samples, cracks have been found only at the notch roots of the 316L samples. There is no evident Hg corrosion observed.

Acknowledgements

The surface analysis work was supported by the Commission of the European Communities under the TMR-Contract No ERB FMRX-CT98-0244 (ESS – European Spallation Source).

References

[1] ESS Council: ESS – A Next Generation Neutron Source for Europe, Volime III: The ESS Technical Study, ISBN 090 237 6 500, November 1996 (Chapter 4).
[2] G.S. Bauer, in: Proceedings of 13th Meeting of the International Collaboration on Advanced Neutron Sources, Villigen PSI, Switzerland, October 1995, p. 547.
[3] J.R. DiStefano, S.J. Pawel, J.H. DeVan, in: Proceedings of the International Workshop on the Technology and Thermal Hydraulics of Heavy Liquid Metals, Schrunce, Austria, March 1996, p. 5.
[4] K. Farrell, L.K. Mansur, International Workshop on Spallation Materials Technology, Oak Ridge, TN, April 1996, p. 3.3-1.
[5] Y. Dai, in: Proceedings of 13th Meeting of the International Collaboration on Advanced Neutron Sources, Villigen PSI, Switzerland, October 1995, p. 604.
[6] J.F. Nejedlik, E.J. Vargo, Electrochem. Technol. 3 (1965) 250.
[7] J.R. Weeks, Corrosion 23 (1967) 96.
[8] J.R. DiStefano, in: Second International Workshop on Spallation Materials Technology, Ancona, Italy, September 1997, p. 247.
[9] Y. Dai, G.S. Bauer, in: M.S. Wechsler, L.K. Mansur, C.L. Snead, W.F. Sommer (Eds.), Materials for Spallation Neutron Sources, The Minerals, Metals and Materials Society, 1998, p. 99.
[10] J.I. Goldstein, D.E. Newbury, P. Echlin, D.C. Joy, C. Fiori, E. Lifshin, Scanning Electron Microscopy and X-Ray Microanalysis, Plenum, New York, 1981.
[11] J. Bénard, Oxidation des metaux, Vol. I, Gauthier-Villas, Paris, 1962.
[12] L.I. Mirkin, Handbook on XRD Analysis of Polycrystals, Publishing House of Physics and Mathematics Literature, Moscow, 1961.
[13] J.J. Gilman (Ed.), The Art and Science of Growing Crystals, Metallurgia, Moscow, 1968.
[14] V.P. Gladyshev, S.A. Levitskya, L.M. Philippova, Analytical Chemistry of Mercury, Nayka, Moscow, 1974.
[15] S. Bretschneider, Properties of Gases and Liquids, Chemistry, Moscow, 1986.
[16] Handbook, Properties of Elements, Metallurgia, Moscow, 1985.